High Bias Voltage Transport in Metallic Single-walled Carbon Nanotubes under Axial Stress

Jürgen Dietel

Institut für Theoretische Physik, Freie Universität Berlin, Arnimallee 14, D-14195 Berlin, Germany

Hagen Kleinert

Institut für Theoretische Physik, Freie Universität Berlin, Arnimallee 14, D-14195 Berlin, Germany and
ICRANeT, Piazzale della Repubblica 1, 10 -65122, Pescara, Italy
(Dated: Received May 3, 2011)

We calculate the current-voltage characteristic of a homogeneously strained metallic carbon nanotube adsorbed on a substrate. The strain generates a gap in the energy spectrum leading to a reduction of the current. In the elastic regime, the current-voltage characteristic shows a large negative differential conductance at bias voltages of around $\gtrsim 0.17$V. We discuss the implications for the current in the superelongated regime.

I. INTRODUCTION

Carbon nanotubes have many electronic and mechanical applications. Their ability to sustain high currents before breaking was observed in a number of experiments on metallic single-walled nanotubes (SWNT) adsorbed on a substrate [1–3]. Corresponding theoretical work was done in Refs. 4, 5. With respect to the mechanical properties, carbon nanotubes belong to the strongest and stiffest materials discovered so far. Under stress, a tube will first expand elastically. After reaching the yield point, it undergoes plastic deformations, leaving a permanent deformation. This point was measured at strains around $5-10\%$ for nanotubes with diameter $1-3$nm depending on the chirality [6, 7].

When the effective temperature of the nanotube caused by the intense electron-phonon scattering at a high bias voltage (we assume in this paper that the system is not externally heated) exceeds the activation barriers of defects, large spiral-like defect stripes are created along the tube [8]. These defect stripes correspond to missing lattice plane pieces in the crystal. The missing atoms of these plane pieces are rearranged at the end points of the nanotube in such a way that a superelongation of SWNTs of up to 270% before cracking is reached. In Ref. 9, we have developed a theory for this effect in a simplified crystal model. Finally, when the effective temperature due to the applied bias voltage is lower than the activation barrier the system responds to the external stress with large non-homogeneous defect pile ups or immediately bond-breaking depending on the physical surrounding [10, 11]. This leads then to necking of the SWNT. Here, we will not address the current-voltage characteristic in this regime.

The purpose of this paper is to analyse the electrical properties in the stress ranges where nanotubes show a homogeneous behavior in space, i.e., in the elastic regime of small elongation, and in the superelongation regime. We will first discuss the elastic regime, and the superelongation regime will be discussed at the end.

If subjected to an external homogeneous stress, a nanotube responds with a homogeneous strain. This results in modifications in the bond lengths and leads, via the electron-phonon interaction, to a gap in the electron spectrum of metallic SWNTs. This strongly modifies the current-voltage characteristic, and represents, therefore, a promising effect for building sensitive stress sensors.

On a substrate, the current increases with voltage, whereas for suspended SWNTs it decreases, i.e., it shows a small negative differential conductance at high voltages [12]. Similarly, we will find here a negative differential conductance which is now very large for a SWNT adsorbed on a substrate under external stress at bias voltages of around 0.17V.

The energy levels of electrons in a nanotube form one-dimensional bands in the graphene Brillouin zone around the **K** and **K**′ points. For metallic SWNTs, there are two energy bands corresponding to right- and left-moving electrons which cross at these points. We assume here that the diameter of the nanotube is so small that electron excitations to higher bands are negligible. For example this approximation is valid at bias voltages $U \lesssim 2$V for nanotubes with diameter 2nm. These diameters are typical in present day current-voltage experiments [1–3]. But we expect the validity of the approximation even beyond this value since electron scattering to higher bands is effectively forward due to the band edges where electrons reverse their direction. Note that we use in our numerical calculations below scattering values for nanotubes with a diameter of 2nm [9].

In order to calculate the current-voltage characteristic at high bias voltage we will use the semi-classical Boltzmann equation for electrons and phonons. The various scattering mechanisms between electrons, phonons and impurities will be discussed first in Sect. II. Then we will discuss in Sect. III the effect of strain on the wavefunctions and the energy spectrum of the electrons in the nanotube. This leads to modifications in the electron-phonon scattering times. Section IV introduces

the different Boltzmann equations for the electrons and phonons which we use in order to calculate the current-voltage characteristic. The results of this calculation will be discuss in Sect. V ending up with a conclusion in Sect. VI.

II. SCATTERING PROCESSES

The method we use here to calculate the current-voltage characteristic of metallic nanotubes is based on the semi-classical Boltzmann equation. Within this method quantum interference corrections to the conductance are not taken into account [13]. It was recently shown numerically that this correction to the conductivity is negligible above room temperature for single-walled carbon nanotubes without structural defects due to phonon scattering decoherence mechanisms [14]. This temperature is immediately reached through electron-optical phonon and further optical phonon-acoustic phonon scattering in nanotubes under high bias voltage.

At low voltages innervalley elastic scattering, which consists of acoustic phonon scattering (in the quasi-elastic limit) and impurity scattering, is most relevant. We neglect electron-electron collisions. At higher voltages inelastic scattering between the electrons and optical phonons, which then leads to intervalley scattering, becomes relevant. This scattering process leads at high bias voltage to the creation of hot optical phonons, which are then no longer in thermal equilibrium with the environment [5]. This leads us to the conclusion that we have to consider besides the electrons also phonons in the semi-classical Boltzmann approach. The hopping between an electron in the **K** valley and the other at the **K**′-valley is mediated by zone-boundary optical A_1' **K**-phonons where only Kekulé type of lattice distortions couple to the electronic system [15]. On the other hand jumps of electrons within the same valley are mediated by zone-center E_{2g} **Γ**-phonons [4]. The optical phonons decay to lower lying secondary acoustic phonons by phonon-phonon scattering [16]. These then decay to other acoustic phonons or phonons in the substrate and to a smaller amount also in the leads. We show in Fig. 1 this electron-phonon relaxation path.

III. STRAIN EFFECTS ON THE ELECTRON SYSTEM

By using the electron-phonon interaction Hamiltonian for acoustic phonons as in Ref. 15 we have calculated the lowest-band eigenfunctions and eigenvalues for a metallic nanotube under stress. For electrons in the **K** valley, these are given by (letting the axis of the SWNT point
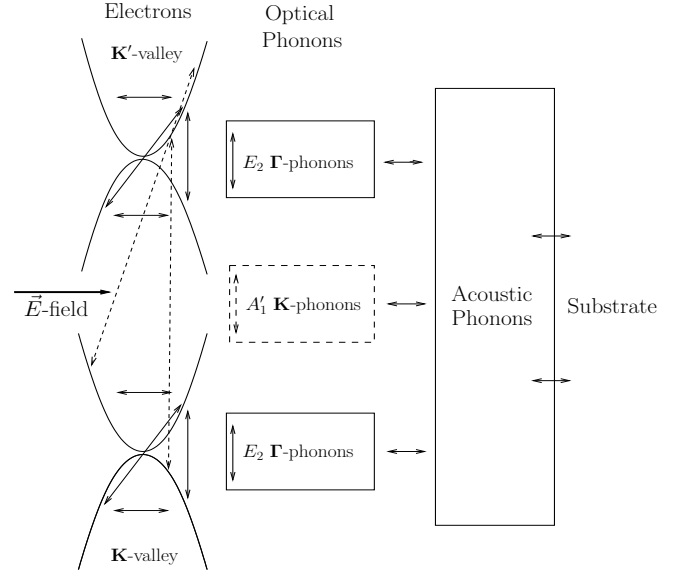

FIG. 1: Main electron-phonon relaxation path of metallic SWNTs at high bias voltage where electron-optical phonon scattering is dominant. Innervalley electron jumps shown as solid doublearrows in the figure are mediated by E_2 **Γ**-phonons. Intervalley electron jumps mediated by A_1' **K**-phonons are shown by dashed doublearrows.

in the y-direction)

$$\Psi_{s,k}^K(y) = e^{iy(k+k_{y_0})} \begin{pmatrix} \frac{k_-}{|k_-|} \\ s \end{pmatrix}, \qquad (1)$$

where $s = 1$ for the conduction band , $s = -1$ for the valence band and k is the momentum in y-direction. Moreover, we used the abbreviation $k_\pm \equiv k_{x_0} \pm ik$ according to

$$k_{x_0} + ik_{y_0} = \frac{g_2}{\hbar v_F} e^{i3\eta} \left[(u_{xx} - u_{yy}) + i2u_{xy} \right]. \qquad (2)$$

Here v_F is the electron velocity, u_{ij} the strain tensor, and $g_2 \sim 2$eV [15] the electron-phonon coupling constant. The parameter η in k_{x_0,y_0} is the chiral angle of the SWNT. For electrons in the **K**′ valley we obtain $\Psi_{s,k}^K(y)$ with the substitution $g_2 \to -g_2$ and $k_{x_0} - ik \to k_{x_0} + ik$.

The energy eigenvalues are

$$\epsilon(s,k) = s\hbar v_F \sqrt{k_{x_0}^2 + k^2}, \qquad (3)$$

Strain makes $k_{x_0} \neq 0$ and opens a gap $\Delta = 2\hbar v_F |k_{x_0}|$ in the electron spectrum of a formerly metallic SWNT. This is consistent with numerical calculations and experiments [17–21]. This spontaneous gap generation is *not* seen by computer calculations in graphene [22]. The energy eigenvalues $\epsilon(s,k)$ show an important exception: The spectrum remains gapless [23, 24] for a metallic SWNT with $\eta = \pi/6$ known as armchair nanotube, where the homogeneous axial stress obeys $u_{xy} = 0$. From this and the discussion below it is clear that armchair nanotubes

show only a small effect on the current-voltage characteristic by an applied external stress. For zigzag SWNTs, for which one has $\eta = 0$, we obtain the maximal gap value for a given applied axial external stress.

Let us now discuss the current-voltage characteristic due to strain. For a formerly metallic nanotube, we obtain that the energy band and the electron-phonon scattering times are modified. Indeed, both depend effectively on the gap parameter Δ which is itself a function of the strain and the chiral angle of the nanotube. We neglect here modifications of the eigenfunctions above due to $k_{y_0} \neq 0$ as this leads effectively only to small momentum shifts of the zone boundary phonon velocities. The corresponding modifications of the current-voltage characteristic are small due to the fact that the effective phonon mean free path is much smaller than the SWNT length. This has been checked numerically. We now discuss the modifications of the effective electron-phonon scattering times due to the wavefunction modifications under stress.

We restrict ourselves first to the **K** valley and zone-center phonon scattering. The results for intervalley scattering are mentioned below Eq. (12). In contrast to the current-voltage characteristic of SWNTs without band gap [5] we have to take backward scattering (inner and interband) and interband forward scattering into account. Interband scattering leads, for example, to the result that the conduction band can be filled with electrons by phonon absorption or depleted by phonon emission. Therefore, we should take into account that we have from the beginning electrons (holes) injected in the conduction (valence) band in the SWNT by a non-zero lead temperature. Without interband scattering, only these electrons and the corresponding holes contribute to the current (see the accompanying discussion to Eq. (13)).

The electronic zone-center phonon scattering Hamiltonian is given by [25]

$$H_{\text{int}} = -\frac{g_3}{a}\begin{pmatrix} 0 & u_y(\mathbf{r}) + iu_x(\mathbf{r}) \\ u_y(\mathbf{r}) - iu_x(\mathbf{r}) & 0 \end{pmatrix}, \quad (4)$$

where a is the nearest-neighbour distance in the lattice and g_3 was determined in Ref. [4] by density functional methods for metallic SWNTs.

Next we calculate the momentum-dependent electron-phonon transition matrix elements $|\langle \Psi_{s,k}^K | H_{\text{int}} | \Psi_{s',k'}^K \rangle|^2$, which are proportional to the effective electron-phonon scattering times. In the following, we mention for which type of phonons, i.e. longitudinal ($u_y \neq 0$ and $u_x = 0$) or transversal ($u_y = 0$ and $u_x \neq 0$), the matrix element $|\langle \Psi_{s,k}^K | H_{\text{int}} | \Psi_{s',k'}^K \rangle|$ is non-vanishing:

$$|\langle \Psi_{s,k>0}^K | H_{\text{int}} | \Psi_{s',k'<0}^K \rangle|^2 \propto \left| k_+/|k_+| + k_-'/|k_-'| \right|^2 \approx 4, (5)$$
$$|\langle \Psi_{s>0,k\gtrless0}^K | H_{\text{int}} | \Psi_{s'<0,k'\gtrless0}^K \rangle|^2 \approx 4. \quad (6)$$

The matrix element (5) comes from interband forward scattering, which means $s \neq s'$, with transverse optical phonons ($u_x \neq 0$). For innerband backward scattering ($u_y \neq 0$),

i.e. $s = s'$, this non-zero matrix element is mediated by longitudinal optical phonons ($u_y \neq 0$). The non-zero matrix element (6) come from interband backward scattering with longitudinal optical phonons ($u_y \neq 0$) if the gap is small ($|k_{x_0}| \ll |k|, |k'|$), and from transversal optical phonons ($u_x \neq 0$) if the gap is large ($|k|, |k'| \ll |k_{x_0}|$). Note that (5) and (6) become exact for large and small gaps and are approximate for intermediate gap values. Note also that in the present approximation, (5), (6), the backward scattering matrix elements do not depend on the stress, i.e., we can set $k_{x_0} = 0$.

IV. CURRENT-VOLTAGE CHARACTERISTIC

In section II we introduced a two-valley model for the scattering mechanisms of the SWNT under bias voltage. In the following, we use the approximation of an effective one-valley model coupled to only one sort of optical phonons. In fact, this was already used by us in Ref. [16] to calculate analytically the current-voltage characteristic of unstrained SWNTs with non-reflecting leads. This is a simplification of the two-valley Boltzmann approach where scattering between the valleys is mediated by zone-boundary and zone-center optical phonons [5, 16] which we discussed in Sect. II. The latter model leads to current-voltage characteristic of unstrained SWNTs [5, 16] which are in good accordance with experiments. Our one-valley approximation is justified by the fact that the optical frequencies of the zone-center phonons and zone-boundary phonons, and also the electron-phonon coupling in the phononic sectors are rather similar. The electron-optical phonon interaction in this model leads to an effective inverse scattering time $1/\tau_{\text{ep}}$ for the electrons and $2s^p/\tau_{\text{ep}}$ for the phonons with parameters found in Ref. 16.

We denote by $f_L(k,x,t)$ $(f_R(k,x,t))$ the left (right) moving electron distribution functions, and by $n^{fs}(k,x,t)$, $n^{bs}(k,x,t)$ the distribution function of the phonons mediating forward or backward scattering of electrons, respectively. The time evolution of the electrons is governed by the semi-classical Boltzmann-equation

$$\left[\partial_t \mp v_e(k)\partial_x + \frac{e\text{E}}{\hbar}\partial_k \right] f_{L/R} = \left[\partial_t f_{L/R} \right]_c. \quad (7)$$

with $v_e(k) = |\partial\epsilon(s,k)/\partial(\hbar k)|$, $[\partial_t f_{L/R}]_c \approx [\partial_t f_{L/R}]_e + [\partial_t f_{L/R}]_{fs} + [\partial_t f_{L/R}]_{bs}$, and elastic scattering

$$[\partial_t f_L]_e = (v_F/l_e)[f_R(k) - f_L(k)]\tilde\nu(\epsilon(s,k)) \quad (8)$$

consisting of acoustic phonon scattering (in the quasi-elastic limit) and impurity scattering where l_e is the elastic scattering mean free path. We denote by $\nu(\epsilon(s,k))$ the density of states of the left or right-moving electrons, i.e. $\nu(\epsilon(s,k)) = 1/|\partial\epsilon(s,k)/\partial k|$ and $\tilde\nu = \nu(\epsilon)\hbar v_F$ is the dimensionless density of states.

The time evolution of optical phonons is given by

$$[\partial_t + v_{\rm op}(k)\partial_x]\, n^{bs/fs} = \left[\partial_t n^{bs/fs}\right]_c + \left[\partial_t n^{bs/fs}\right]_{\rm osc}.$$
(9)

Here $v_{\rm op}$ is the optical phonon velocity [16]. $\left[\partial_t n^{bs/fs}\right]_c$ is a phonon-electron scattering term consisting of the interaction with backward or forward scattered electrons. $\left[\partial_t n^{bs/fs}\right]_{\rm osc}$ is a thermal phonon relaxation term such

that the coupled electron-phonon system is not heated up by applying large voltages on the SWNT.

Scattering of phonons with electrons leads to the following scattering contributions (backward scattering and forward interband scattering) in the electronic Boltzmann equation (7) and in the phononic Boltzmann equation (9) (we restrict ourselves to $k > 0$ phonons in (11) for simplicity)

$$[\partial_t f_L]_{bs/fs}(k,x) =$$
(10)
$$\frac{1}{\tau_{\rm ep}}\Bigg(\tilde\nu(\epsilon^+)r^{bs/fs}(\epsilon^+)\Big\{[n^{bs/fs}(k^+,x)+1]f_{R/L}(k_{R/L}(\epsilon^+))[1-f_L(k_L(\epsilon))]-n^{bs/fs}(k^+,x)[1-f_{R/L}(k_{R/L}(\epsilon^+))]f_L(k_L(\epsilon))\Big\}$$
$$+\tilde\nu(\epsilon^-)r^{bs/fs}(\epsilon^-)\Big\{n^{bs/fs}(-k^-,x)f_{R/L}(k_{R/L}(\epsilon^-))[1-f_L(k_L(\epsilon))]-[n^{bs/fs}(-k^-,x)+1][1-f_{R/L}(k_{R/L}(\epsilon^-))]f_L(k_L(\epsilon))\Big\}\Bigg),$$

$$\left[\partial_t n^{bs/fs}\right]_c(k,x) = 2\frac{s^p}{\tau_{\rm ep}}\left|\frac{1}{\tilde\nu(\epsilon(k_L^+))}\pm\frac{1}{\tilde\nu(\epsilon(k_L^-))}\right|^{-1}\Bigg([n^{bs/fs}(k,x)+1]\Big\{f_R(k_R^+)[1-f_{L/R}(k_{L/R}^-)]$$
(11)
$$+f_{L/R}(-k_{L/R}^-)[1-f_R(-k_R^+)]\Big\}-n^{bs/fs}(k,x)\Big\{f_{L/R}(k_{L/R}^-)[1-f_R(k_R^+)]+f_R(-k_R^+)[1-f_{L/R}(-k_{L/R}^-)]\Big\}\Bigg)$$

with the abbreviations $k^\pm = k_R(\epsilon^\pm)-k_L(\epsilon)$, $\epsilon^\pm = \epsilon\pm\hbar\omega$ in (10). In (11) we used the abbreviation

$$k_{R/L}^\pm = \pm\frac{k}{2}+\frac{\omega}{2v_F}\sqrt{\frac{\frac{\omega^2}{v_F^2}-k^2-4k_{x_0}^2}{\frac{\omega^2}{v_F^2}-k^2}}.$$
(12)

where the right hand side of Eq. (12) is independent of R, L and k is the phonon momentum. The numerical constant s^p is given by $s^p \approx 0.67$ [16]. The frequency of the optical phonon is denoted by ω. The factors $r^{bs/fs}(\epsilon^\pm)$ within our one-valley model are determined by the influence of zone-boundary $\mathbf{K}$-phonon scattering on the effective electron-phonon scattering time by carrying out a similar overlap calculation for these phonons as was done for zone-center $\mathbf{\Gamma}$ phonons below Eq. (6). Here we use the zone-boundary phonon scattering Hamiltonian in Ref. 26 together with similar approximations used below Eq. (6). This leads to $r^{bs}(\epsilon^\pm) \approx 0.7(1/\tilde\nu(\epsilon^\pm)+1/\tilde\nu(\epsilon))^2/4+0.3$ for backward scattering and $r^{fs} \approx 0.3$ for interband forward scattering [16].

We restrict ourselves here to short SWNTs with lengths between 50nm where phonon scattering becomes relevant and 500nm. For the thermal phonon relaxation term $\left[\partial_t n^{bs/fs}\right]_{\rm osc}$ we use an expression which takes into account also the second generation acoustic phonons with parameters discussed in the case of the metallic SWNTs without external stress in Ref. 16. Since $|1/\tilde\nu(\epsilon(k_L^+)) - 1/\tilde\nu(\epsilon(k_L^-))|^{-1} \gg 1$ in (11) we can disregard, in the calculation of Eq. (9), the term $\left[\partial_t n^{fs}\right]_{\rm osc}$, and the term $v_{\rm op}(k)\partial_x n^{fs}$ for the forward scattering phonons. To inte-

grate the Boltzmann equations (7)-(11) we use a generalisation of a discretized time-splitting method described in Ref. 16 for the stress-free case. Due to the change in the density of states coming from the external stress, the momentum and space-grid is no longer equidistant in position space but still equidistant in momentum space [27]. The large prefactor $|1/\tilde\nu(\epsilon(k_L^+)) - 1/\tilde\nu(\epsilon(k_L^-))|^{-1}$ in (11) allows us to determine $\partial_t n^{fs}$ in every iteration process by (11) with $\left[\partial_t n^{fs}\right]_c(k,x) = 0$. This dynamics leads approximately to the same stationary solution of (7), (9) as in the case when using the full phonon scattering dynamics (11).

V. DISCUSSION

The upper panel in Fig. 2 with the continuous curves shows the current-voltage characteristic calculated with the help of (7)-(11) for a SWNT of length $L = 300$nm and different values of the gap energies Δ. Note that the black circles are calculated for gap energies $\Delta \to 0$ just after the gap opening. The recorded data points are restricted by the demand that the momentum grid, the energy values Δ and optical phonon frequencies ω are commensurate. By comparing the current values I for voltage $U = 1.5$V and very small gap energy $\Delta \to 0$ with the corresponding values for metallic SWNTs [5, 16] we obtain that the current values are around a factor six times smaller after the gap is opened. The crosses at the curves in Fig. 2 shown for $\Delta < \hbar\omega$ are calculated
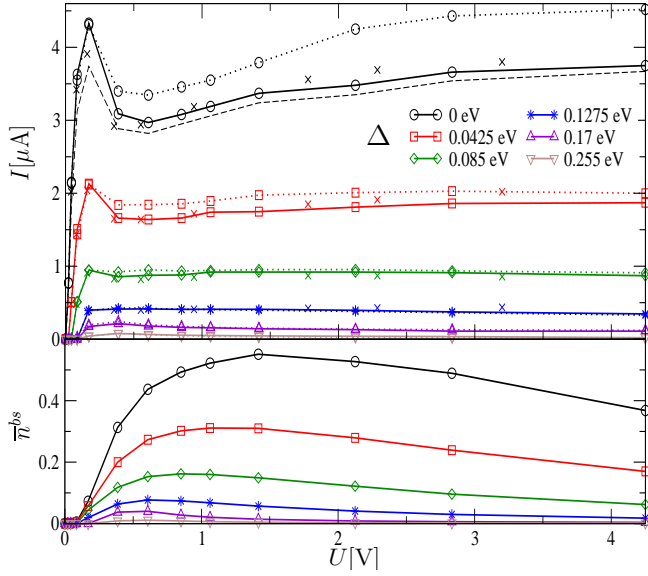
FIG. 2: (Color online) Upper panel with the continuous curves shows the current-voltage curve obtained using (7)-(9) for a nanotube of length $L = 300$ nm, $l_e = 1600$ nm [2, 5, 16] and various gap energies Δ. The dashed curve is calculated for $\Delta \to 0$ and $l_e = 800$nm. The crosses uses the full two electron band, three phonon type theory with exact transition matrix elements. The dotted curves uses GW parameter values within the one-valley model for the electron-optical phonon scattering time [30]. The lower panel shows the corresponding momentum and position averaged backward scattering phonon distribution function $\overline{n}^{bs}$ defined in Ref. 16.

using the full two electron valley model coupled to E_{2g} $\mathbf{\Gamma}$-phonons as well as A_1' $\mathbf{K}$-phonons where we used now the exact electron-phonon transition matrix elements in our numerics shown at the left hand side in (5) and (6) for the $\mathbf{\Gamma}$-phonons. We used here parameter values given in Refs. [4, 5, 16] and further that the phonon velocities of the transversal $\mathbf{\Gamma}$-phonons is minus half of the velocity of the longitudinal ones [28].

In the lower panel in Fig. 2 we show the corresponding energy-position averaged backward phonon distribution function $\overline{n}^{bs}$ [16] (7)-(11). We obtain that the phonon distribution function is around three to four times smaller for a SWNT after gap opening at 1.5V when comparing it with the phonon distribution function values of the corresponding metallic nanotube [4, 16].

Figure 3 shows the current-voltage characteristic of a metallic SWNT where just the gap is opened, i.e. $\Delta \to 0$, for various nanotube lengths. Here we recorded more data points. We obtain a dip in the current-voltage characteristic with a large negative differential conductance for $U \gtrsim \hbar\omega/e$ by taking into account that $\hbar\omega \approx 0.17$eV. Fig. 2 shows that this behavior survives even at much smaller elastic scattering lengths. We can understand this dip in the current curve in the following way: For small voltages $k_B T/e \ll U \ll \hbar\omega/e$, phonon scattering can be neglected and the total current is the sum of the
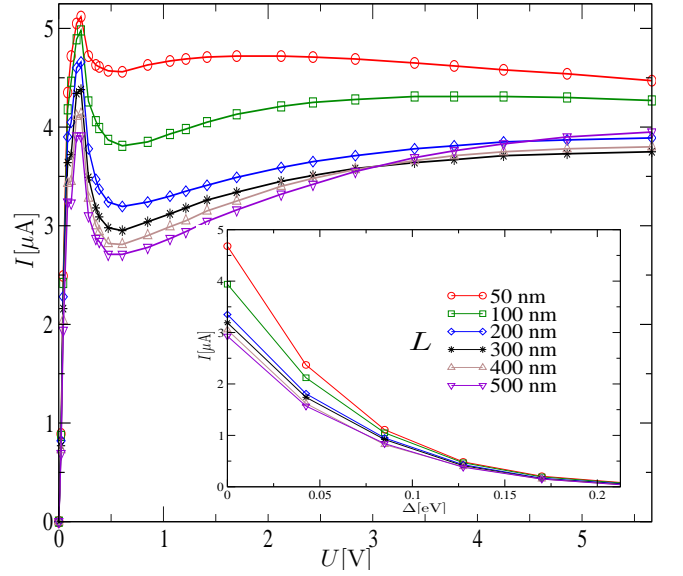

FIG. 3: (Color online) We show the current-voltage curve for SWNTs with a gap $\Delta \to 0$ and certain SWNT lengths L ($l_e = 1600$nm). The inset shows the current curve for a voltage $U = 1V$ and several nanotube lengths L as a function of the gap energy Δ.

currents in each band separately. This current is for general Δ approximately given by

$$I_0 = \frac{8e}{h} \int_{\Delta/2}^{\infty} d\epsilon\, n_F(\epsilon) = \frac{8e}{h} k_B T \left\{ \ln\left[1 + \exp\left(\frac{\tilde{\Delta}}{2}\right)\right] - \frac{\tilde{\Delta}}{2} \right\}.$$

(13)

with $\tilde{\Delta} \equiv \Delta/k_B T$ and n_F is the Fermi-function. At room temperature $T \approx 300$K and small gaps $\Delta \to 0$ we have $I_0 \approx 5.3\mu$A. We point out that I_0 is independent of the length L of the SWNT. In (13) we neglect elastic scattering, which is only a small correction factor since $L/l_e \ll 1$ for small SWNTs [16]. In the following discussion it is useful to have in mind that the energy broadening $K_B T$ of the electrons (holes) in the conduction (valence) band is much smaller than the phonon frequency at room temperature, i.e. $k_B T/\hbar\omega \sim 0.14$. At higher voltages $U \gtrsim \hbar\omega/e$ first interband scattering starts. Due to the electron distribution function factors in the phonon scattering terms in (10) and (11) interband backward scattering from the conduction band to the valence band is then the dominant scattering contribution. This leads to a reduction of the current I_0 of order $I_r^{U\sim\omega} \sim (e/h)k_B T L/l_{\rm ep}$ where the electron-phonon mean free path is given by $l_{\rm ep} = v_F \tau_{\rm ep} \approx 130$nm [16]. At even higher voltages $U \gg \hbar\omega/e$ also innerband scattering starts. This leads to an energy diffusion of the electrons (holes) in the conduction (valence) band with an energy broadening from $\Delta\epsilon \sim k_B T$ without scattering to $\Delta\epsilon \sim (\hbar\omega/\pi)(1 + L/l_{\rm ep})$ for $eU \gtrsim (\hbar\omega/\pi)(1 + L/l_{\rm ep})$ [16]. This broader energy band consists of equally spaced

subbands with separation distance $\hbar\omega$ and energy width $\sim k_B T$. This follows from $k_B T \ll \hbar\omega$ and by taking into account the energy conservation in the electron-phonon scattering process. In this voltage regime the reduction of I_0 due to interband scattering is changed to $I_r^{U \gg \omega} \sim (e/h)(k_B T/\pi)(1 + L/l_{\rm ep})(\hbar\omega/eU)L/l_{\rm ep}$. This leads to a vanishing of interband scattering at high voltages shown in Fig. 3 as a dip in the current-voltage characteristic with negative differential conductance. From Fig. 3 we obtain that the considerations above are true only for $L \ll 500$nm. For $L \approx 500$nm we obtain a saturation of the depth and the width of the voltage dip. The reason lies in the fact that at larger nanotube lengths also secondary scattering processes like interband scattering from the valence band to the conduction band has to be taken into account which was not done in the scaling considerations above. Also the phonon density dependence of the effective electron-phonon scattering length $l_{\rm ep}$ [16] should be included.

At even higher voltages we obtain from Fig. 3 that $\lim_{U \to \infty} I \approx I_0$ (apart from elastic scattering). This shows that a current reduction due to innerband scattering is very small in this regime. Phonons which are created by electron scattering in one band can only scatter electrons in the other band on a length $\Delta x \sim L(1 + L/l_{\rm ep})(\hbar\omega/eU)/\pi$ so that we can consider the Boltzmann system (7)-(11) in each band separately at high voltages. This leads to the result that the electrons (holes) are effectively down (up) scattered in the conduction (valence) band. Then, by taking into account the fact of existing band edges near the Fermi-niveau for small stresses, we obtain that innerband scattering does not influence the absolute current at high voltages.

The inset in Fig. 3 shows the current-voltage curve for a SWNT at bias voltage $U = 1$ V for various nanotube lengths as a function of the gap energy Δ. The functional behavior of the reduction factor from the $\Delta \to 0$ current value is reproduced well by Eq. (13).

Recently, it was shown for graphene [29, 30] that screening effects in the electron-electron interaction are relevant for the calculation of the zone-boundary electron-phonon scattering time. In Ref. 30 a numerical Green's function method (GW) was used in contrast to the standard density functional (DFT) theory in order to calculate this scattering time. Note that our one-valley model used so far is based on scattering parameters obtained by the latter calculation. The calculated values within the GW method are in better agreement with the experimentally obtained energy dispersion of the zone-boundary phonons for graphene than the values of the DFT calculation. For the zone-center phonons the agreement is less satisfactory with the experiments than in the DFT-method [31, 32]. To our knowledge up to now in contrast to the DFT calculations for SWNTs in Ref. [4] an explicit GW calculation for the electron-phonon scattering time in carbon nanotubes is still missing. Since electron screening is highly dimension dependent this calculation would be of course of general interest. Neverthe-less we are now able to calculate from Ref. [30] within the GW method by using the zone-folding method [4] effective electron-phonon scattering times for zone-center and zone-boundary phonon scattering for SWNTs. By using Mathiessen rule we obtain an effective electron-phonon scattering length $l_{\rm ep} = 68$nm for an SWNT with diameter 2nm. Corresponding scattering times for the phonons due to electron-phonon scattering, the averaged phonon frequencies and phonon velocity for the one-valley model can be calculated accordingly by using the definitions in Ref. 16. The acoustic-optical phonon scattering ratio $\tau_{\rm ac}/p\tau_{\rm op}$ [16] is then determined from the theoretical determined current-voltage characteristic of the full two-valley model by comparison with the experimentally given current-voltage characteristic for the $L = 300$nm SWNT without stress. We obtain values $\tau_{\rm ac}/p\tau_{\rm op} = 3.5$ for an optimal accordance to the differential conductance at high voltages. The absolute theoretical current-value is then around 20% lower in the high voltage regime than in the experiment. By using these theoretical GW quantities we show by the dotted curves in the upper panel in Fig. 1 the current-voltage characteristic for a $L = 300$nm SWNT and various gap energies Δ within an effective one-valley model.

Up to now we only considered metallic nanotubes. Semiconducting nanotubes show already a gap Δ without stress. Since $\Delta \gg \hbar\omega$ for small diameter semiconducting SWNTs (~ 2nm) we obtain a vanishingly small current-voltage curve in this case. For semiconducting tubes with much larger diameters, the energy gap Δ is decreasing but in order to obtain quantitatively the current-voltage characteristic one should take into account also the much larger electron-phonon scattering time $\tau_{\rm ep}$ [4] of such systems and further that now also higher transversal electron bands become important. Nevertheless, we expect from the discussion above a qualitative similar current-voltage behavior, with a negative differential conductance at $U \gtrsim \hbar\omega/e$ as for the metallic nanotubes. Similar should be true for graphene nanoribbons. Remember that the existence of a negative differential conductance region in the current-voltage characteristic is mainly based on the gap opening under stress and that we have $k_B T \ll \hbar\omega$ at room temperature. Here we note that corresponding to armchair nanotubes discussed above metallic zigzag-edged nanoribbons do not show a gap opening under axial stress in contrast to armchair edged ones. This is shown by numerical calculations in Ref. 33 based on an atomistic model. This follows also immediately from the electron-phonon interaction Hamiltonian for acoustic phonons in Ref. 15 which we used above in the derivation of (1) and (2).

Finally, we briefly discuss the current-voltage characteristic of a SWNT in the superelongation regime. In Ref. 9 we obtain that with increasing external stress defect stripes are created with increasing lengths for increasing stress. This is seen by a kink motion at the boundary surface of the SWNT in transmission electron microscope pictures [8]. The number of these stripes is

proportional to the external stress whose lengths corresponds to missing lattice plane pieces in the crystal. In first approximation we expect that the current is given by the electrons running over complete lattice planes. The electrons which run over incomplete lattice planes are completely backscattered and these do not contribute to the current. For those electrons which run over the complete lattice planes we further have to consider the linear elasticity current corrections which we have discussed at length above. All this means that for armchair SWNTs, which do not show a stress dependent gap we expect a linear decreasing current curve as a function of the external stress. Such a behavior is in fact experimentally observed in Ref. 8.

VI. CONCLUSION

We have calculated the current-voltage characteristic of metallic carbon nanotubes under homogeneous axial stress in the linear elastic regime lying on a substrate by means of a semi-empirical Boltzmann equation for electrons and phonons. We have found that the stress leads to an energy gap which, causes a large negative differential conductance at $U \gtrsim \hbar\omega/e$. Moreover this negative differential conductance is largest at small stress just after the gap is opened, getting smaller with a larger stress applied. Materials with such a behavior are very useful for the activation and deattenuation of oscillating circuits. For larger voltages at $U \approx 1.5V$ and small stress just after the gap opening we obtain approximately six times smaller current values for the $L = 300$nm nanotube in comparison to the tube without stress. The corresponding momentum and position averaged optical phonon distribution function is around three to four times smaller. In addition to the discussion of the current-voltage characteristic in the linear elastic regime we have also discussed modifications of the characteristic in the superelongation regime.

Concerning the current-voltage characteristic of large diameter semiconducting nanotubes and graphene nanoribbon, we have argued that a qualitative similar differential negative behaviour as for the metallic nanotube should be seen.

[1] Z. Yao, C. L. Kane, and C. Dekker, Phys. Rev. Lett. **84**, 2941 (2000).

[2] J. Y. Park, S. Rosenblatt, Y. Yaish, V. Sazonova, H. stnel, S. Braig, T. A. Arias, P. W. Brouwer, and P. L. McEuen, Nano Letters **4**, 517 (2004).

[3] A. Javey, J. Guo, M. Paulsson, Q. Wang, D. Mann, M. Lundstrom, and H. Dai, Phys. Rev. Lett. **92**, 106804 (2004).

[4] M. Lazzeri, S. Piscanec, F. Mauri, A. C. Ferrari, and J. Robertson, Phys. Rev. Lett. **95**, 236802 (2005).

[5] M. Lazzeri and F. Mauri, Phys. Rev. B **73**, 165419 (2006).

[6] P. Zhang, P. E. Lammert,V. H. Crespi, Phys. Rev. Lett. **81**, 5346 (1998).

[7] D. Bozovic, M. Bockrath, J. H. Hafner, C. M. Lieber, and H. Park, M. Tinkham, Phys. Rev. Rev. B **67**, 033407 (2003).

[8] J. Y. Huang, S. Chen, Z. Q. Wang, K. Kempa, Y .M Wang, S .H. Jo, G. Chen, M. S. Dresselhaus, Z. F.Ren, Nature **439**, 281 (2006).

[9] J. Dietel and H. Kleinert, Phys. Rev. B **79**, 245415 (2009).

[10] B. I. Yakobson, M. P. Campbell, C. J. Brabec, and J. Bernholc, Comput. Mater. Sci. **8**, 341 (1997).

[11] M. B. Nardelli, B. I. Yakobson, and J Bernolc, Phys. Rev. Lett. **81**, 4656, (1998).

[12] E. Pop, D. Mann, J. Cao, Q. Wang, K. Goodson, and H. Dai, Phys. Rev. Lett. **95**, 155505 (2005).

[13] S. Datta *Electronic Transport in Mesoscopic Systems*, (Cambridge University Press, Cambridge, 1995).

[14] H. Ishii, S. Roche, N. Kobayashi, and K. Hirose, Phys. Rev. Lett. **104**, 116801 (2010).

[15] H. Suzuura and T. Ando, Phys. Rev. B **65**, 235412 (2002).

[16] J. Dietel and H. Kleinert, Phys. Rev. B **82**, 195437 (2010).

[17] L. Yang and J. Han, Phys. Rev. Lett **85**, 154 (2000).

[18] E. D. Minot, Y. Yaish, V. Sazonova, J.Y. Park, M. Brink, and P. L. McEuen, Phys. Rev. Lett **90**, 156401 (2003).

[19] J. Cao, Q. Wang, and H. Dai, Phys. Rev. Lett **90**, 157601 (2003).

[20] A. G. Souza Filho, N. Kobayashi, J. Jiang, A. Grüneis, R. Saito, S. B. Cronin, J. Mendes Filho, Ge. G. Samsonidze, G. Dresselhaus, and M. S. Dresselhaus, Phys. Rev. Lett **95**, 217403 (2005).

[21] M. Huang, Y. Wu, B. Chandra, H. Yan, Y. Shan, T. F. Heinz, and J. Hone, Phys. Rev. Lett. **100**, 136803 (2008).

[22] F. M. D. Pellegrino, G. G. N. Angilella, and R. Pucci, Phys. Rev. B **81**, 035411 (2010).

[23] L. Yang, M. P. Anantram, J. Han, and J. P. Lu, Phys. Rev. B **60**, 13874 (1999).

[24] A. Maiti, A. Svizhenko, and M. P. Anantram, Phys. Rev. Lett. **88**, 126805 (2002).

[25] K. Ishikawa and T. Ando, J. Phys. Soc. Jpn. **75**, 084713 (2006).

[26] H. Suzuura and T. Ando, J. Phys. Soc. Jpn. **77**, 044703 (2008).

[27] Our space grid is the same, while our momentum grid is twice as large as in the stress-free calculations of Ref. [16].

[28] J. Maultzsch, S. Reich, C. Thomsen, H. Requardt, and P. Ordejón, Phys. Rev. Lett. **92**, 075501 (2004).

[29] D. M. Basko and I. L. Aleiner, Phys. Rev. B **77**, 041409(R) (2008).

[30] M. Lazzeri, C. Attaccalite, L. Wirtz, and F. Mauri, Phys. Rev. B **78**, 081406(R) (2008).

[31] S. Piscanec, M. Lazzeri, F. Mauri, A. C. Ferrari, and J. Robertson, Phys. Rev. Lett. **93**, 185503 (2004).

[32] M. Lazzeri, S. Piscanec, F. Mauri, A. C. Ferrari, and J. Robertson, Phys. Rev. B **73**, 155426 (2006).

[33] M. Poetschke, C. G. Rocha, L. E. F. Foa Torres, S. Roche, and G. Cuniberti, Phys. Rev. B **81**, 193404 (2010).